Study of 3D-printed onyx parts reinforced with continuous glass fibers: Focus on mechanical characterization, analytical prediction and numerical simulation

Daouda Nikiema, Pascale Balland, Alain Sergent

Accepted Manuscript

Cite as:

D. Nikiema, P. Balland, A. Sergent, Study of 3D-printed onyx parts reinforced with continuous glass fibers : Focus on mechanical characterization , analytical prediction and numerical simulation, 0 (2024) 1–20. https://doi.org/10.1177/00219983241247913.

Study of 3D-Printed Onyx Parts Reinforced with Continuous Glass Fibers: Focus on Mechanical Characterization, Analytical Prediction and Numerical Simulation

Daouda Nikiema; Pascale Balland; Alain Sergent

Université Savoie Mont Blanc, SYMME, F-74000 Annecy, France

Corresponding author: Daouda Nikiema

Email: daouda.nikiema@univ-smb.fr; daoudanikiema94@gmail.com

Phone/Fax: +33 4 50 09 65 67/+33 4 50 09 65 43

Abstract

The 3D printing of continuous-fiber composites is currently relevant to engineers and researchers. This study aims to characterize and predict the mechanical properties of Onyx/glass fiber specimens printed using 3D printing. The work assesses the impact of glass fiber printing parameters on the mechanical behavior of printed parts and proposes analytical and numerical methods to predict mechanical properties. A physicochemical analysis was conducted on 3D printed continuous glass fibers. The study also investigated the impact of fiber printing parameters on composite parts. The results indicate that the 3D-printed glass fibers consist of nylon, continuous glass fibers, and voids (porosity), which range from 58% to 63%, 31% to 38%, and 5% to 8%, respectively. Mechanical characterizations indicate that printing fiber layers in blocks results in superior mechanical properties compared to printing alternating layers of glass fibers and Onyx. Additionally, the concentric mode of fiber printing can be challenging if the 'start rotation' parameter is not adjusted correctly. Premature specimen breakage occurred when fiber printing began within their useful length, resulting in a deformation at break that was approximately 34% less, depending on the starting position. The proposed analytical and numerical prediction methods had prediction errors of approximately 7% to 12% and 5% to 7%, respectively. Engineers can use these prediction approaches during the dimensioning phase of 3D printed composite parts.

Keywords: 3D printing; continuous glass fiber composites; Elastic modulus; Numerical simulation; Mechanical behavior.

1 Introduction

3D printing emerged in the late 1980s as a technique for creating objects layer by layer from their 3D representation. Nowadays, this manufacturing technique is utilized in various sectors, including transportation (automotive, rail, and aerospace), the medical field [1], and more recently, the construction industry [2]. The reduction of waste generated during production and the increased capacity to produce complex components are the main advantages of this manufacturing process over traditional methods [3,4]. Historically, plastic filament-based printers have been the most widely utilized. However, continuous technological advancements have seen the emergence of innovative, high-performance printers that can produce fiber-reinforced or composite parts [5,6].

The fibers used as reinforcements in 3D printing composites are often short or long. Nylon, Polylactic Acid (PLA), Thermoplastic Polyurethane (TPU), and Acrylonitrile Butadiene Styrene (ABS) are commonly employed plastic materials in 3D printing [7–9]. These plastic materials do not inherently exhibit good mechanical properties. Applying a heat treatment to the printed parts can improve the mechanical properties of these thermoplastics [10]. Additionally, the mechanical performance of parts can be enhanced by adding short or long fibers or particles (powder). In a study, Kumar et al. [11] demonstrated that the inclusion of wood or iron oxide powder can enhance specific mechanical properties, such as toughness, during recycling cycles. Lupone et al. [12] showed that the continuous carbon fiber filament has significantly superior mechanical properties compared to nylon filament. Similarly, Fernandes et al. [13] reported an elastic modulus of 39.35 GPa and 1.75 GPa for an Onyx specimen reinforced with continuous carbon fibers versus an Onyx-only specimen. Brenken et al. [14] reported in a literature review that weak points of 3D printing short-fiber composites were related to fiber damage during printing, void formation between layers, and poor mechanical performance in the transverse direction of the parts. The authors also demonstrated that mechanical strength equivalent to that of aluminum can be achieved when parts are reinforced with continuous fibers. The authors concluded that, despite the limitations, the 3D printing process for composites holds great potential. Continuous-fiber printers are growing in popularity in academic literature compared to other printer types, such as plastics and short-fiber composites. Recently, a literature review was conducted by Tian et al. [15], concentrating on the enhancements and uses of 3D printing utilizing long-fiber composites. The mechanical properties of the commonly used continuous fibers, carbon, and glass were investigated in a previous study by Justo et al. [16]. In addition to the two fibers mentioned above, Al Abadi et al. [17] extended this research by including Kevlar fibers in their studies. Kabir et al. [18] confirmed in a literature review that adding continuous fibers to 3D printed parts significantly improves their mechanical properties. They also noted a growing interest in this process, as evidenced by the high number of publications on 3D printing of composites. Mechanical characterization of these composites soon became a significant concern for the scientific community.

As with any manufacturing process, conducting a mechanical characterization of parts obtained through the 3D composite printing process and studying printing parameters and their influence on the mechanical properties of printed parts has become crucial. In a study by Li et al. [19], the mechanical properties of thermoplastic specimens (specifically, Polyamide 6 or PA6) were characterized through tension, compression, 3-point bending, and impact testing. These specimens

were reinforced with long carbon fibers. The researchers discovered a significant impact of fiber printing techniques on the mechanical properties of the printed parts. The specimens exhibited multiple failure mechanisms, such as fiber pull-out, fiber/matrix delamination, and fiber/matrix breakage. Chen and colleagues [20] fabricated a continuous carbon fiber filament (CCF) impregnated with polyether ketone (PEEK) and investigated the mechanical properties of specimens produced with this novel CCF/PEEK filament based on various printing parameters. Their findings demonstrated that enhancing the nozzle temperature and printing bed while reducing the printing speed and layer thickness significantly improved the tensile strength of the specimens. In their study, Saeed et al. [21] investigated the tensile and flexural properties of polyamide specimens that were reinforced with continuous carbon fibers. They found that increasing the volume of carbon fibers resulted in improved mechanical strength and modulus of the specimens. Furthermore, they demonstrated that utilizing a high-temperature press to press the specimens enhanced their mechanical properties. Similarly, the study by Ali et al. [22] demonstrated that a specimen featuring a triangular print pattern (at a 50% fill density) reinforced with carbon fibers exhibited superior mechanical properties compared to specimens with rectangular or hexagonal print patterns. They also investigated the impact of specimen printing orientation and discovered that lateral orientation resulted in a higher Young's modulus and tensile strength when compared to a flat orientation. Sanei et al. [23] compiled a list of continuous fiber printing parameters that can affect the mechanical properties of parts in a literature review. They also provided a list that demonstrates the significance of each printing parameter on the mechanical performance of parts. For instance, they showed that concentric fiber printing is used to optimize the mechanical properties of parts. Araya-Calvo et al. [24] also confirmed in their study that concentric fiber printing improves the mechanical compressive performance of parts. Sanei et al. [25] demonstrated that concentric fibers can reduce the impact of stress concentration and prevent breakage in these regions. Yu et al. [26] also showed that specimens printed with concentric fibers had the best flexural mechanical properties and better energy absorption than specimens printed with isotropic fibers. In their study, Mohammadizadeh et al. [27] demonstrated that the isotropic printing mode with fiber inclusion offered the best mechanical properties for parts. The main failure modes of the specimens were identified as fiber pull-out and fiber breakage. Given the complexity of the 3D printing process and the various printing parameters involved, it's clear that using analytical prediction methods and numerical simulation to predict the mechanical properties and behavior of printed parts is a major challenge. Overcoming this challenge is necessary to reduce the number of mechanical tests required and to move closer to optimizing the process.

Conventional composite manufacturing processes have inspired analytical methods for predicting the mechanical properties of 3D-printed composites. The most commonly employed method in literature is the rule of mixtures (ROM). Through a study of composites containing glass, carbon, and Kevlar fibers in varying volumes, Díaz-Rodríguez et al. [28] verified the method's predictive abilities. In [29], researchers utilized ROM and found prediction errors ranging from 0% to 60% when compared to tests. Other commonly used methods include volume average stiffness (VAS) and classical laminate theory (CLT). Lupone et al. [12] found prediction errors ranging from 2.2-12.4%, 0.9-8.4%, and 2.3-5.9%, respectively, for ROM, VAS, and CLT. Numerous approaches exist in the literature for predicting mechanical properties and behaviors through numerical simulation. The conventional approach for numerically simulating composites involves 2D Shell elements, which were employed in [30]. Krzikalla et al. [31] compared four types of models, which were mainly composed of 3D elements and 2D shell elements with isotropic and transverse isotropic behavior models. Their findings revealed that modeling using shell and 3D elements reinforced with 1D elements yielded accurate predictions with an average error of 3% compared to bending tests. More recently, Avanzini et al. [32] used embedded elements and 2D shell elements to predict the stiffness of nylon specimens that were reinforced with

continuous carbon fibers. Their research revealed the effectiveness of both modeling methods in predicting specimen stiffness. Prior research on 3D printed composites concentrated on characterizing and predicting mechanical properties, with little emphasis on fiber printing parameters.

The literature review indicates that there is a great deal of interest in the 3D printing of continuous fiber composites by researchers and engineers. However, some aspects of the process have not been adequately studied and require further investigation. This will ultimately lead to a better understanding of the process. Firstly, questions relating to the materials used in terms of their physicochemical compositions and microstructure (porosity studies) have not been addressed. Secondly, questions concerning fiber printing parameters have not been sufficiently studied to identify their influences on printed parts. Lastly, the analytical and numerical models proposed in the literature for some of them generate a large discrepancy between predicted and experimental results. In this work, a study of the physicochemical composition of continuous glass fibers is carried out in order to identify the different constituents and their respective proportions by volume. This study is the first novelty of this work. Next, a study of the main fiber printing parameters will be carried out to identify their potential influences on the mechanical performance of printed parts. Finally, analytical and numerical models are presented to predict the behavior and mechanical properties of the composites. The key feature of these predictive models will be the separate consideration of the different parts of the composite parts. In order to carry out this work, the manuscript has been divided into three parts: the first part deals with the material and the method, the second part presents the results and discussions, and the final part draws conclusions and outlines the prospects for the work.

2 Material and method

2.1 3D printer, material, and sample design

The Marforged X7 printer from the American manufacturer Marforged was utilized in this study. It features a dual printing nozzle capable of printing thermoplastic components, either reinforced or unreinforced, with continuous fibers. The printer can accommodate a print volume of up to 330 mm x 270 mm x 200 mm and has a print resolution ranging from 50 µm to 250 µm.

The printer is compatible with various thermoplastic materials developed by the manufacturer, including Onyx, FR Onyx (flame retardant), FR-A Onyx (flame retardant - aeronautic), white nylon, and PLA (polylactic acid). These materials can be reinforced with continuous glass, carbon, or Kevlar fibers. The Eiger slicing software provides access to multiple printing parameters, such as solid, triangular, hexagonal, rectangular, and gyroid printing patterns with variable densities and layer thickness. In addition, it offers options for concentric or isotropic fiber placement modes, allowing users to specify the fiber orientation angle in 0.1-degree increments.

In this research, the thermoplastic material utilized is Onyx. As per the manufacturer and earlier studies [33], Onyx filament has a diameter of 1.75 mm and comprises polyamide 6 (nylon) mixed with short carbon fibers ranging between 10% and 20% by volume, as presented in Figure 1 (a). While printing, these short fibers are mainly oriented in the printing direction, resulting in superior mechanical strength of the printed parts.

The glass fibers employed in this analysis serve as continuous reinforcement. The nylon coating on these fibers melts during printing, adhering to the Onyx and promoting interlayer adhesion. Figure 1 (b) depicts the various components within the glass fiber filament.

The printed and tested specimens were designed using CAD software (Inventor Educational Version 2022). The rectangular cross-section of the specimens is shown in Figure 2, with the dimensions conforming to the following standards (ASTM D638 and ASTM D3039) while still accommodating the

tensile machine utilized in this research. The ASTM D638 standard was initially used for mechanical tensile testing. However, it was discovered that the shape of the test specimens was unsuitable as fractures were observed in the jaws of the tensile testing machine. To address this issue, the geometric shape of the test specimens was modified in accordance with ASTM D3039, allowing the specimens to break within their useful length. Table 1 provides an overview of the general printing parameters employed throughout the study.

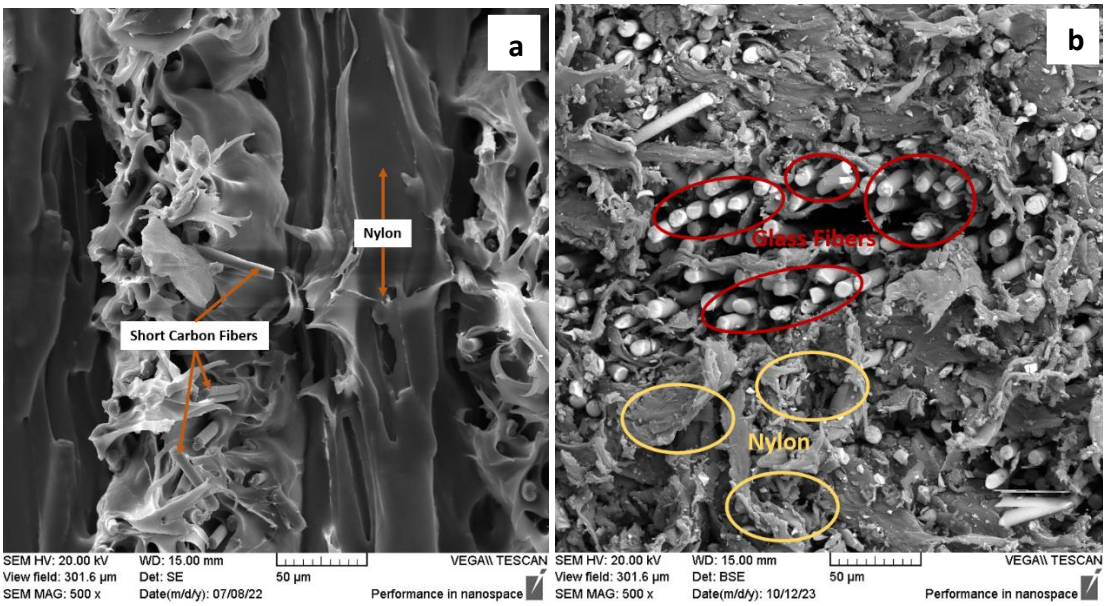

Figure 1: Scanning electron microscope (SEM) image: a) Onyx; b) 3D-printed glass fiber

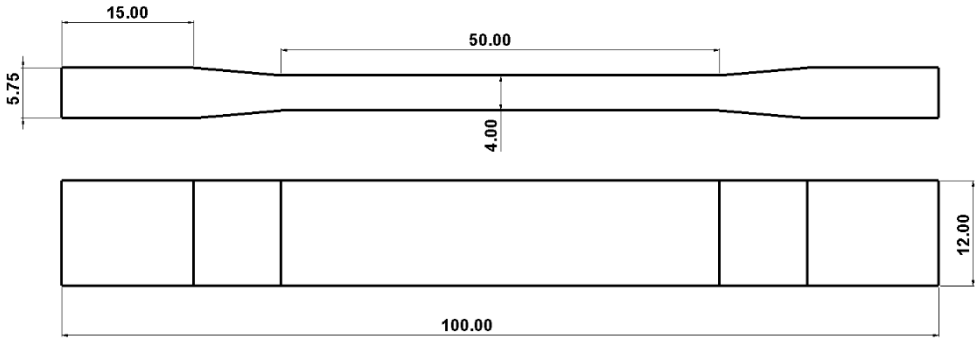

Figure 2: Sample geometry (dimensions in millimeters)

Table 1. General printing setting in this study

Printing parameters	Specifications
Thermoplastic - Fibers	Onyx – Glass fibers
Pattern - density	Solid - 100%
Layer thickness – wall width (mm)	0.1 – 0.4
Fiber deposition mode	Isotropic / Concentric
Walls (contours) count	2 to 6
Plastic – Fiber nozzle temperature (°C)	273 – 250

2.2 Glass-fiber layer stacking mode

Glass fiber-reinforced Onyx specimens were analyzed to investigate the impact of fiber layer positioning on specimen height. A specimen with 12 glass fiber layers was printed in three sequences. The first sequence involved layering the glass fiber and Onyx alternately (1Lx12), shown in Figure 3 (a). The second sequence consisted of specimens made of two blocks of glass fiber layers separated by Onyx layers. Each block comprises six layers of glass fiber, as denoted by the notation 6Lx2 and illustrated in Figure 3 (b). In the final sequence, the fibers were printed as a single block in the center of the specimen section, labeled 12Lx1, and shown in Figure 3 (c).

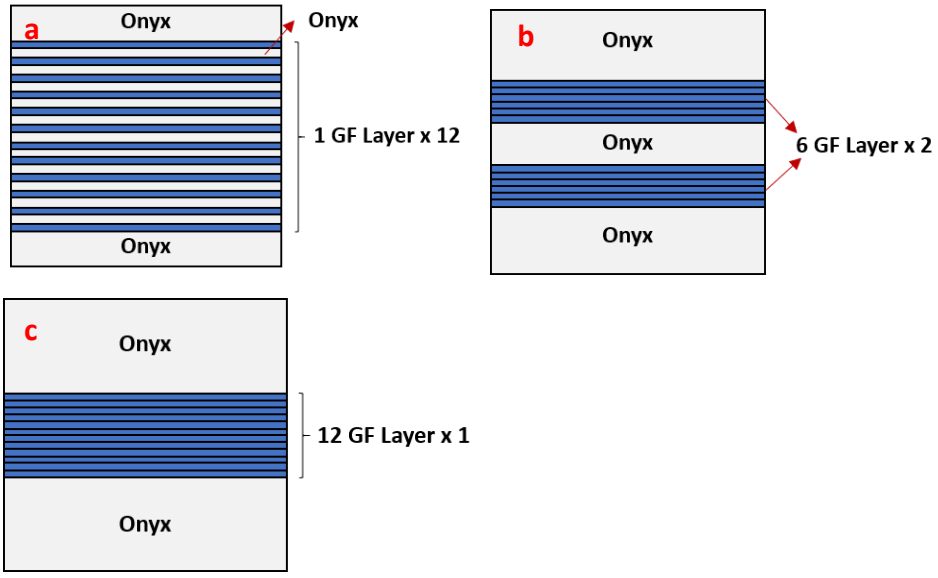

Figure 3: Different arrangements of glass fiber in the composite samples: a) 1L x 12; b) 6L x 2; c) 12L x 1.

2.3 Fiber printing mode

The Marforged X7 printer provides numerous options for 3D printing composites. There are two main modes when printing fibers: concentric and isotropic, depicted in Figure 4 (a) and Figure 4 (b), respectively. In concentric mode, the trajectory revolves around the geometric shape of the component to be printed. In isotropic mode (not to be confused with the isotropic behavior of a material), the user can select various angles at which to print the fibers during setup, allowing for greater flexibility.

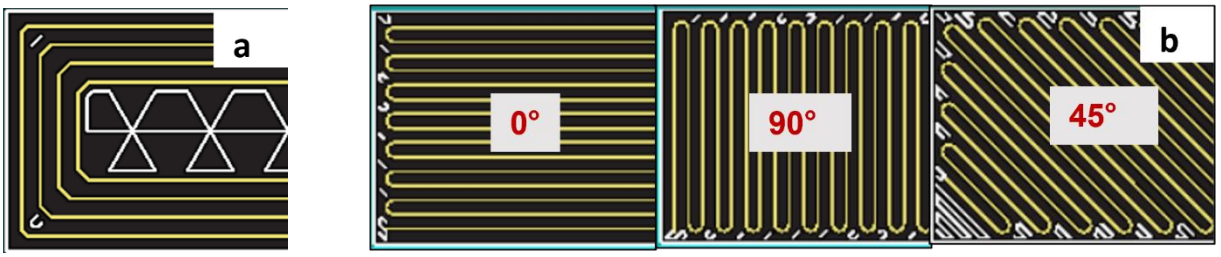

Figure 4: Fiber-reinforcing mode: a) concentric mode; b) isotropic mode (fibers at 0°, 90°, and 45°).

2.3.1 Concentric printing mode

The concentric mode presents a range of parameters, including the number of fiber bands (strips), number of fibers per band, number of concentric fibers, and start rotation percentage, determining the point at which fiber printing begins. Figure 5 (a) and Figure 5 (b) depict these parameters. This section will solely focus on fiber start position (start rotation) to evaluate its impact on the mechanical

properties of printed parts. As illustrated in Figure 5 (b), three different print start positions were investigated.

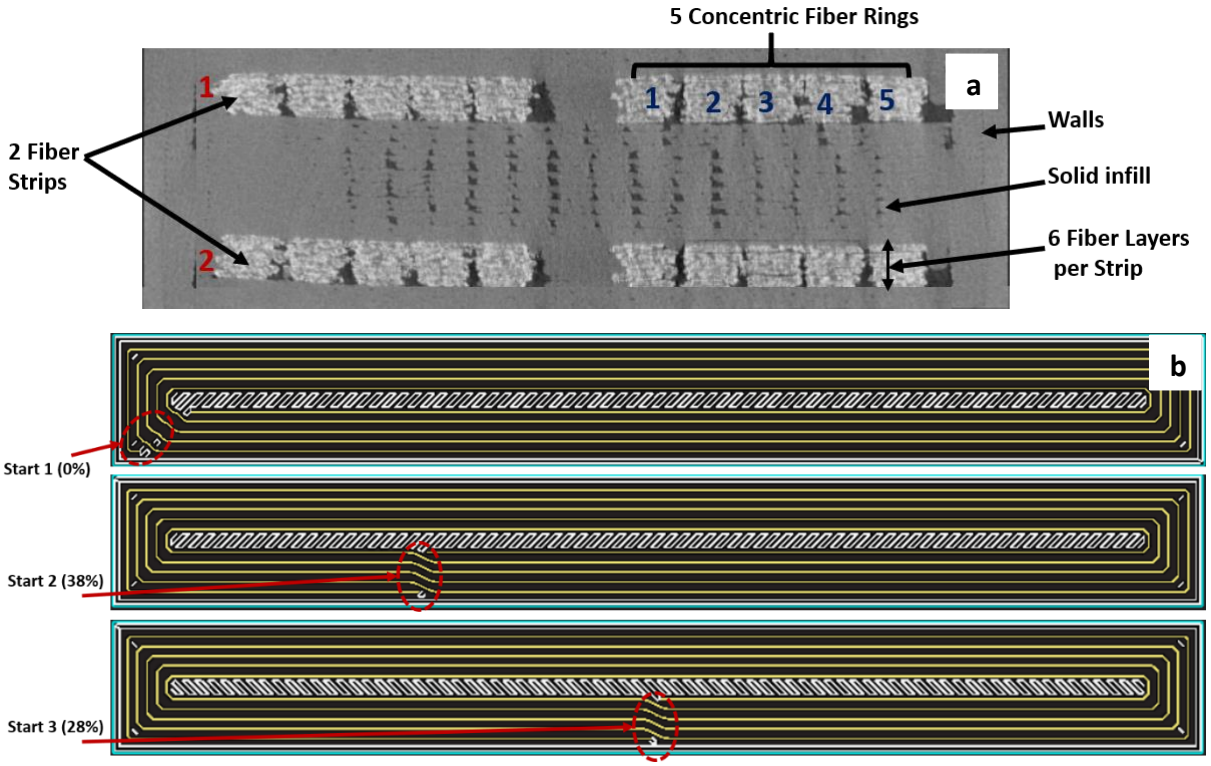

Figure 5: Concentric mode. a) cross-section of the concentric sample. (X-ray tomographic image); b) concentric samples studied (Start1: the fibers start printing in the unstressed areas of the specimen; Start2 and Start3: the fibers start printing in the stressed area of the specimen).

2.3.2 Isotropic printing mode

The isotropic mode differs significantly from the concentric mode, allowing fibers to be printed at varying orientation angles (the angle increment allowed by Eiger is 0.1 degree). The user can define the orientation of the fiber layers based on their technical requirements. This printing mode bears similarities with the traditional composite manufacturing methods. The specimen investigated in this section was 3D printed with fibers oriented at 0°, +45°, -45°, and 90°. This investigation explores analytical tools that can predict mechanical properties and determine the most suitable tools for 3D-printed composites. The specimen studied had 16 layers of glass fibers, which corresponded to a 33% fiber volume. The configuration for the fibers was [0/+45/-45/90]2S, as depicted in Figure 6. The number of Onyx walls specified for this section is two.

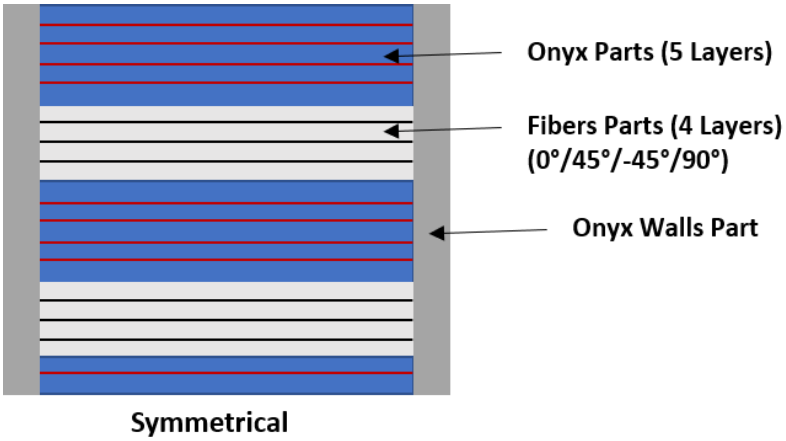

Figure 6: Cross-section of specimen studied with isotropic printing mode.

2.4 Experimental tensile tests

The experimental tests performed in this study consisted exclusively of tensile tests performed on a universal tensile testing machine (Instron-5569) equipped with a 50 kN load cell and an extensometer with an initial length of 12.5 mm and a maximum strain of +/- 40%, at a test speed of 10 mm/min. Each test necessitated a minimum of three specimens, and the mean mechanical characteristics were computed. The experiments were conducted solely on glass fiber samples and composite specimens (Onyx + glass fiber). The Young's modulus is the main mechanical property calculated according to ASTM D3039. It is expressed by the following formula (1):

$$E = \frac{\sigma_2 - \sigma_1}{\varepsilon_2 - \varepsilon_1} \quad (1)$$

where σ_1 and σ_2 represent the stress for a strain of $\varepsilon_1 = 0.1\%$ and $\varepsilon_2 = 0.3\%$, respectively.

2.5 Volume ratio and porosities study of printed glass fiber

The printed glass fibers consist of continuous glass fibers and nylon; however, the volume ratios of these components are not provided by the manufacturer, Markforged. To ascertain these ratios as well as the porosity of the printed glass fibers, two techniques have been employed: one destructive based on ASTM D3171 and one non-destructive based on X-ray tomographic.

First method based on ASTM D3171 is an experimental approach to determine the volume ratio of the different constituents. The experiment involves dissolving glass fiber specimens in a sulfuric acid solution to determine the volume ratio of glass fibers, nylon, and void (porosity).

The second method, which is non-destructive, uses X-ray tomographic analysis to determine the void ratio in printed glass fiber specimens. This involves passing each specimen through the tomograph to obtain images required for analysis using ImageJ software (an open-source software)

2.6 Analytical and numerical predictions of mechanical properties

The present study proposes predicting the mechanical properties of 3D-printed composites using two main approaches: an analytical approach and a numerical approach. The analytical approach employs four methods: the rule of mixtures (RoM), the volume-averaged stiffness method (VAS), the classical laminate theory (CLT), and the so-called 10% method. The primary objective of these analytical methods is to forecast the Young's modulus of the specimens based on the selected printing configurations.

A numerical approach was utilized to predict the Young's modulus of the specimens and their overall behavior under tensile loading. Two numerical simulation methods were used:

- 2D Shell Element Simulation: This simulation type is commonly used for composite modeling. It takes into consideration all the elastic mechanical parameters for every component of the composite, including fibers, the Onyx (infill), and walls (Table 2). The glass fiber layers were modeled with transverse isotropic mechanical behavior characterized by elastic parameters: $\boldsymbol{E_1 = 24\ GPa}$, $\boldsymbol{E_2 = 0.8\ GPa}$, $\boldsymbol{G_{12} = 1\ GPa}$ and $\boldsymbol{\nu_{12} = 0.25}$. Meshing was carried out utilizing SR4 (Shell 4 node reduced integration) finite elements. A mesh convergence study was conducted to eliminate the influence of element size on numerical results. The element size used was approximately 0.4 mm per element.

- Embedded Element Simulation: This modeling technique utilizes 3D elements to represent Onyx and walls, with 1D wire elements representing fibers. The Material properties of the different elements are delineated in Table 2. Its greatest advantage is its ability to recreate even complex fiber trajectories accurately. In Abaqus, the "host part" corresponds to the Onyx, while the fibers are represented by "embedded elements." The host part is meshed with 3D finite elements using C3D8R (an 8-node, reduced-integration brick element), while the embedded part is meshed with 1D finite elements using B31 (a 2-node beam element). After conducting the mesh convergence study, it was determined that the optimal element size is approximately 0.4 mm for volume elements and 0.2 mm for 1D elements. Additional information and steps for performing this simulation can be found in references [32] and [34].

Table 2. Material parameters used in numerical simulations.

	Glass fibers	**Onyx (infill)**	**Onyx (Walls)**
Elastic modulus (GPa)	70	1.66	5.4
Poisson's ratio	0.25	0.35	0.35
Hollomon plasticity (K ; n)	-	63.63 ; 0.148	142.5 ; 0.142
Glass fiber shape and dimensions			
Cross-section shape	**Width**		**Thickness**
Rectangular	0.57 mm		0.052 mm

3 Results and discussion

This section presents results from tensile tests performed on pure glass fiber and composite specimens. Additionally, it includes a discussion and presentation of porosity values and the calculation of the Young's Modulus for glass fibers. The printing modes of the fibers are presented, followed by analytical and numerical simulation approaches that are analyzed. Finally, an approach is presented to optimize the mechanical properties of 3D-printed composites.

3.1 Tensile test results

3.1.1 Pure glass-fibers

Printing a specimen made solely from fiberglass is not yet possible on the Markforged X7 printer. Therefore, to overcome this issue, a single bottom layer of Onyx and a wall were added to the printed specimen and removed prior to testing. These tests aimed to investigate the tensile modulus of fiberglass specimens by altering the number of fiber layers (i.e., specimen thickness). To achieve this, the specimens under examination consisted of 7, 14, and 20 layers of glass fiber, respectively. These specimens are named 7FGL, 14FGL, and 20FGL, as shown in Figure 7.

Figure 7: 3D printed glass fiber samples.

The stress-strain curves of the tested specimens and the comparison of their tensile modulus are presented in Figure 8, demonstrating practically identical curves and tensile modulus regardless of the number of layers or specimen thickness. As a result, the mechanical properties of the glass fiber samples are not affected by this factor, i.e. the mechanical properties of the samples are not affected by the number of layers printed when the fiber printing parameters remain constant for all layers. These results are consistent with the literature, specifically with the findings of Marșavina et al. [35], who demonstrated that the Young's modulus of specimens printed with 4 mm and 10 mm thickness is not significantly affected by specimen geometry, i.e., specimen thickness.

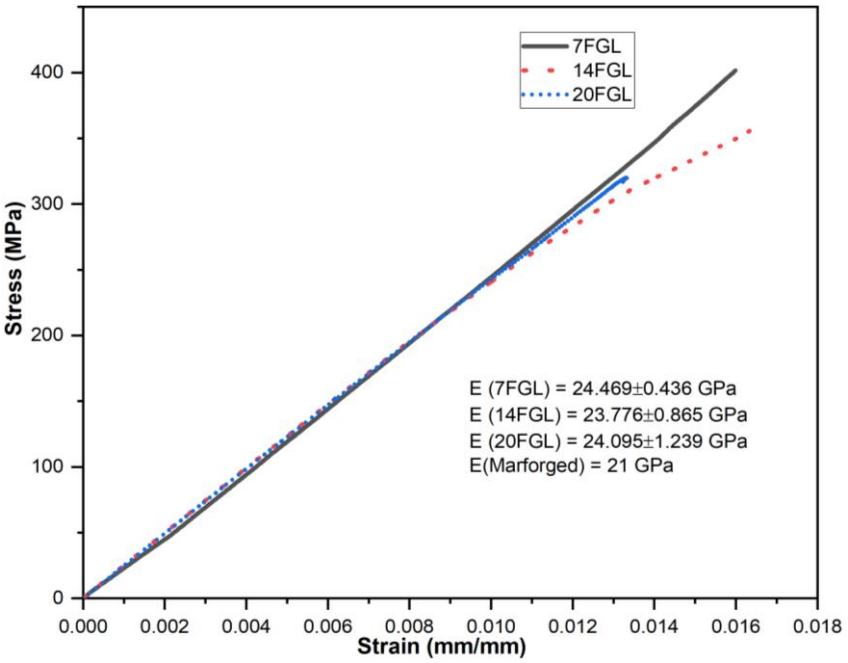

Figure 8: Tensile test curves of glass fiber samples according to the number of layers.

3.1.2 Influence of glass-fiber stacking mode

The three distinct modes of stacking the glass fiber layers within the Onyx composite were investigated. The results of the tensile tests indicate a slight variation in the elastic modulus values among the three printing sequences. Specifically, the elastic modulus for sequence 1Lx12, 6Lx2, and 12Lx1 are 8.313±0.546 GPa, 8.553±0.257 GPa, and 9.229±0.158 GPa, respectively. It appears that the first sequence yields a lower Young's modulus than the other two sequences. The printing configuration that yields optimal results involves grouping the glass fiber layers as closely together as possible, rather than printing them successively with Onyx material between two glass fiber layers. This is likely due to inadequate adhesion between Onyx and glass fibers. Printing several layers of fiber and alternating them with Onyx increases the number of contact surfaces between the two materials. It is important

to note that this may result in weaker adhesion between the glass fiber and Onyx, leading to a potentially weaker specimen compared to fewer contact surfaces. However, block printing the fibers reduces the number of contact surfaces, resulting in a specimen with significantly greater mechanical strength. These observations and conclusions are consistent with those of other studies [24,36], which showed poor adhesion between fibers and plastic layers and good mechanical performance when fibers were grouped as a block rather than alternating with plastic layers.

3.2 Porosities of 3D printed glass fibers and effective properties

Two techniques, one destructive (acid attack) and one non-destructive (X-ray tomographic), have been used to determine the porosity of printed glass fibers. Figure 9 displays an image of the glass fibers after they were dissolved and dried. Based on ASTM D3171, the volume ratios of the different constituents were computed using equations (2) to (4). Calculations were made for specimens at 0°, +/- 45°, and 90°, with six samples obtained per test. Mean values and standard deviations were subsequently determined.

Figure 9: 3D printed glass fibers after acid digestion of nylon and other constituents.

$$\%V_{fiber} = 100 * \left(\frac{m_2 * \rho_1}{m_1 * \rho_2}\right) \quad (2)$$

$$\%V_{resin} = 100 * \left(\frac{m_1 - m_2}{m_2} \times \frac{\rho_1}{\rho_3}\right) \quad (3)$$

$$\%V_{void} = 100 - (\%V_{fiber} + \%V_{resin}) \quad (4)$$

With, m_1: mass of the printed glass fiber sample, m_2: mass of glass fibers after acid attack. ρ_1: density of glass fibers (2.58 $g.cm^{-3}$), ρ_2: density of printed glass fibers (1.5 $g.cm^{-3}$), ρ_3: density of nylon resin (1.1 $g.cm^{-3}$).

The test results indicate that 3D-printed glass fiber specimens typically contain between 31 - 33% glass fibers by volume, 58 - 63% resin (nylon) by volume, and 5 - 8% void by volume, as illustrated in Figure 10. It is evident that the fiber printing angle does not have a significant impact on the void %. These new findings contrast with those of Delbart et al. [37], who previously demonstrated the influence of printing angle and layer thickness on the porosity of PLA-printed specimens. The literature generally reports varying glass fiber contents ranging from 31.5% to 38%, depending on the chosen method [38].

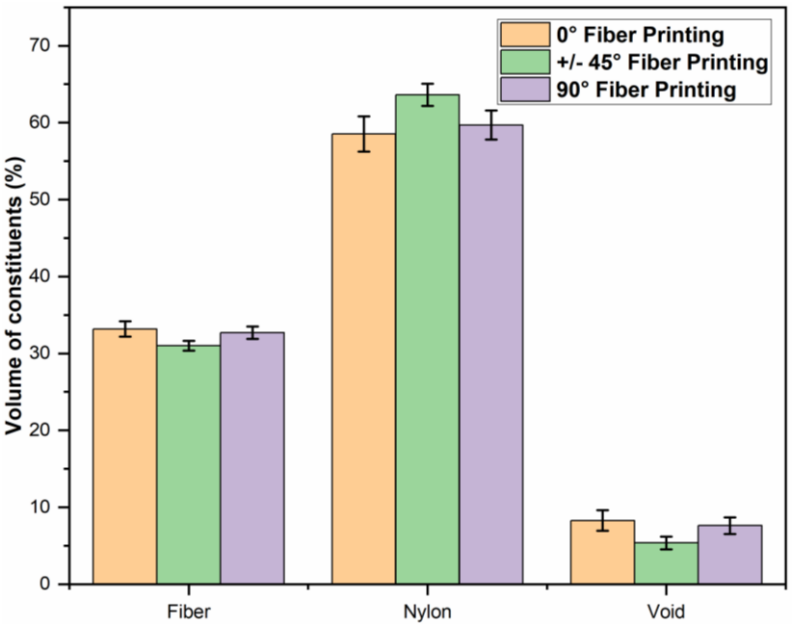

Figure 10: Volume ratio of each constituent of 3D printed glass fiber filament.

The tomographic analyses revealed void ratios that are similar to those obtained through the acid digestion method. The only disadvantage of the tomographic method is that it doesn't provide the resin ratio. However, it has the advantage of being non-destructive, a feature that the sulfuric acid method lacks. This method is destructive, but it provides the ratio of each component. Figure 11 displays a comparison between the two methods.

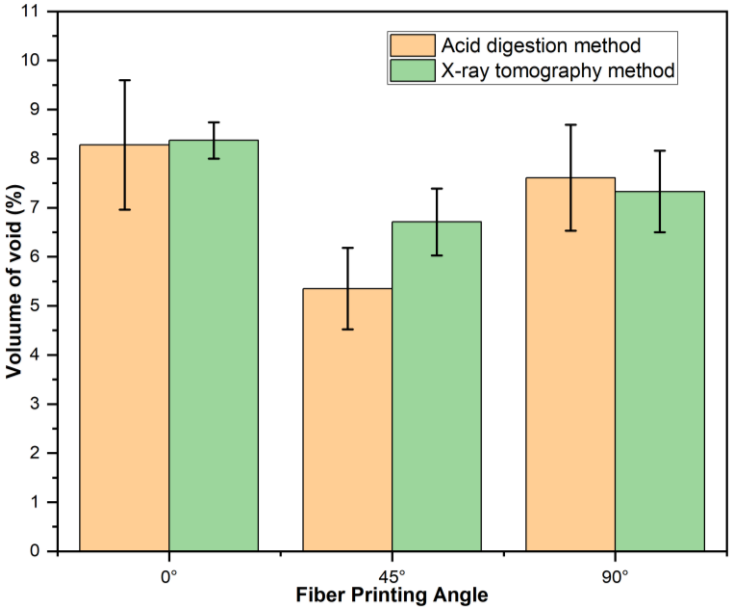

Figure 11: Comparison of void volume obtained by methods 1 and 2 according to fiber printing angle.

Knowing the ratio of glass fibers enables us to compute their effective properties using equation (5):

$$E_{fiber} = (E_{PGF} - E_{nylon} * \%V_{nylon})/\%V_{fiber} \quad (5)$$

Here, E_{PGF} represents the elastic modulus of printed glass fibers with a value of 2.4 GPa, while E_{nylon} is the elastic modulus of nylon as specified by the manufacturer, amounting to 1.7 GPa. Moreover, $\%V_{nylon} = 0.59$ corresponds to the proportion of resin (nylon) present in the glass fiber filament and

$\%V_{fiber} = 0.33$ is the proportion of effective fibers present in the glass fiber filament. The calculated value of the elastic modulus for the glass fibers is approximately $E_{fiber} = 70\ GPa$, similar to values reported in the literature [39]. Knowing the precise value of the elastic modulus is crucial for its use in numerical simulations. Figure 12 (a) and Figure 12 (b) depict the initial cross-section of the printed glass fibers and the effective cross-section determined from the porosity calculation. Together, expressions (6) through (9) are employed to determine the effective dimensions of the glass fibers. The original printed cross-section (A_{PGF}) is rectangular, illustrated in Figure 12 (a), with the assumption that the effective glass fibers can be collected into a singular glass fiber of rectangular cross-section (A_{fiber}), displayed in Figure 12 (b).

$$A_{PGF} = a * b \tag{6}$$

Considering the fiber ratio, the cross-section of the fiber can be determined using equation (7).

$$A_{fiber} = \%V_{fiber} * A_{PGF} = c * d \tag{7}$$

Where c and d are the fictitious dimensions defined for the equivalent glass fiber. By incorporating equation (7) into equation (8), expression (9) can be used to calculate the dimensions c and d. For both dimensions of the equivalent fiber, the same geometric form factor of $\sqrt{\%V_{fiber}}$ was employed.

$$A_{fiber} = c * d = \%V_{fiber} * a * b = \left(a * \sqrt{\%V_{fiber}}\right) * \left(b * \sqrt{\%V_{fiber}}\right) \tag{8}$$

$$c = \left(a * \sqrt{\%V_{fiber}}\right) \text{ and } d = \left(b * \sqrt{\%V_{fiber}}\right) \tag{9}$$

The calculated dimensions are $c = 0.052\ mm$ and $d = 0.57\ mm$ with a fiber ratio of $\%V_{fiber} = 0.33$. These dimensions will be used for the numerical simulation with the embedded elements in section 3.5 of the paper.

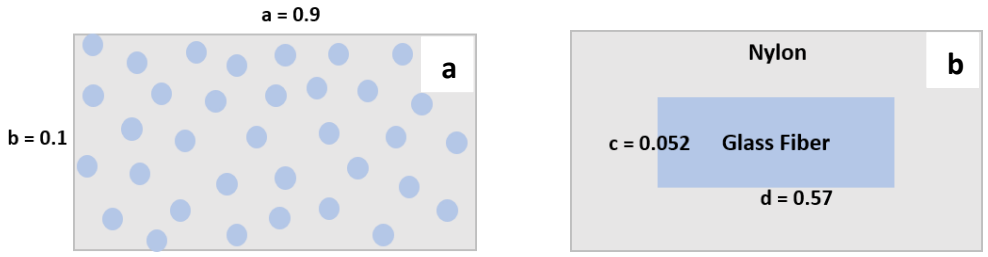

Figure 12: Printed glass fiber section and equivalent glass fiber section (dimensions in millimeters).

3.3 Fiber printing mode

3.3.1 Concentric printing mode

The tensile curves and Young's modulus values for the concentric samples are shown in Figure 13 and Table 3, respectively.

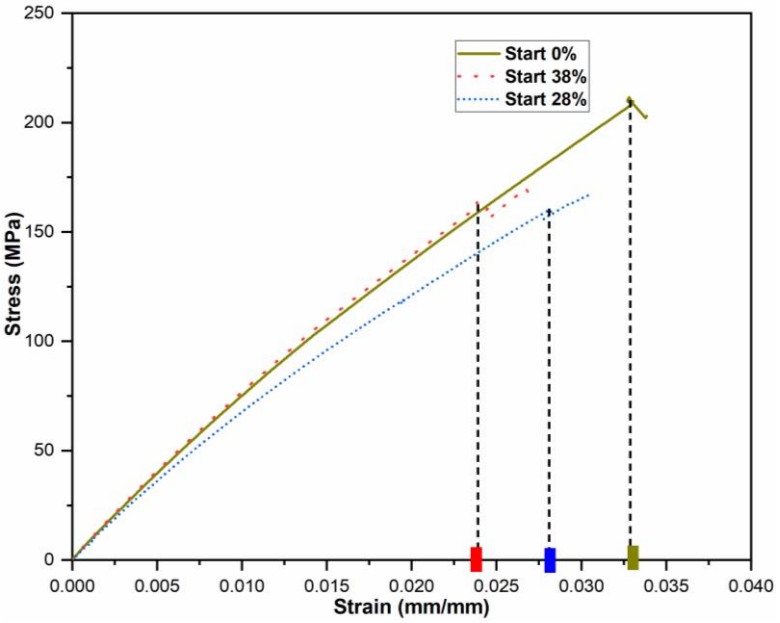

Figure 13: Tensile test curves for concentric samples according to start rotation value.

Table 3. Elastic modulus for concentric samples according to start rotation value.

	Start1	Start2	Start3
E1 (GPa)	8.542	8.623	7.123
E2 (GPa)	8.113	8.044	7.539
E3 (GPa)	7.893	8.090	7.655
Average (GPa)	8.182	8.252	7.439
Standard Deviation	0.330	0.321	0.279

The results showed that if the start of fiber is within the useful length of the specimen, there is a high probability of premature specimen failure. For example, the elongation at break of the Start1 specimen is approximately 3.5%, while the elongation at break of the Start2 and Start3 specimens are 2.3% and 2.8%, respectively (approximately 34% less elongation). These results clearly demonstrate the premature failure of specimens whose fibers begin within their useful length. Melenka et al. [40] mention that parts tend to fail at the point where the fibers begin to imprint due to stress concentrations. The analysis of the elastic modulus (Young's modulus) does not show any significant difference between these specimens. A maximum difference of about 10% was observed between the different Young's moduli. Finally, the "start rotation" parameter is a key parameter to be considered in part design. The values of this parameter must be adjusted to position the start of fiber printing in the least stressed areas of the part to minimize the risk of premature failure.

3.3.2 Isotropic printing mode

The tensile curve of the specimen displayed in Figure 14 closely resembles the results of all three tests, which is further affirmed by the low value of standard deviation on the elastic modulus (E). The mean elastic modulus is determined to be 5121 MPa with a standard deviation of 195 MPa. In comparison, Goh et al. [41] reported an elastic modulus of roughly 7200 MPa for a composite consisting of 35% by volume of unidirectional glass fibers at 0°. Thus, this proves that 0° unidirectional fibers possess greater rigidity than differently oriented fibers.

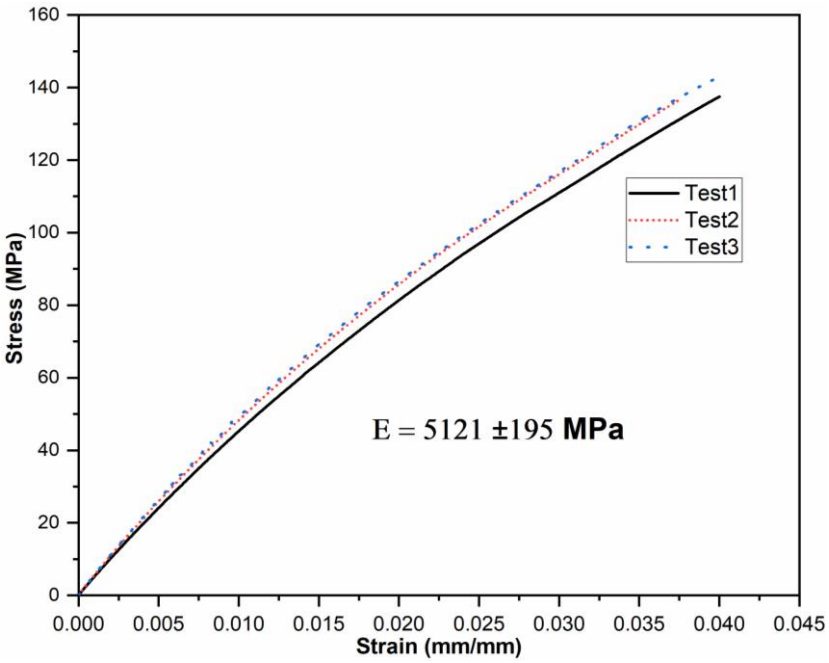

Figure 14: Tensile test curves of a specimen studied with the isotropic printing mode.

3.4 Analytical prediction of the mechanical properties of 3D-printed composites

Analyzing the mechanical properties of 3D-printed composite parts is crucial for manufacturers and users. This section explores four analytical methods for predicting the elastic modulus, focusing on the specimen studied in the previous section (section 3.3.2). The Onyx elastic parameters utilized in this analysis are summarized in Table 4 and previously characterized in [42], and the elastic parameters of the fibers were obtained by mechanical testing.

Table 4. Elastic parameters used for analytical and numerical predictions

	Printed glass fibers	**Onyx (solid part)**	**Onyx (walls parts)**
Longitudinal modulus E1 (GPa)	24	1.66	5.4
Transversal modulus E2 (GPa)	0.8	1.66	5.4
Poisson's ratio v12	0.25	0.35	0.35
In-plane shear modulus G12 (GPa)	1	0.615	2
Volume ratio (V)	$V_{PGF} = 0.33$	$V_{onyx} = 0.54$	$V_{walls} = 0.13$

3.4.1 Rule of mixture with Krenchel coefficient

The first model uses the widely accepted law of mixtures (ROM) from the literature to predict the mechanical properties of composites. A new factor, the "Krenchel coefficient (n_0)," is introduced, which takes into account the fiber orientation angle. The elastic modulus of the composite is calculated through equation (10).

$$E = n_0 E_{PGF} V_{PGF} + E_{onyx} V_{onyx} + E_{walls} V_{walls} \quad (10)$$

Where, E_{PGF} is the elastic modulus of the printed glass fibers, V_{PGF} is its volume ratio, E_{onyx} is the elastic modulus of Onyx, V_{onyx} is its volume ratio, E_{walls} is the elastic modulus of walls, and V_{walls} is its volume ratio. The values of all these parameters are shown in Table 4. The Krenchel coefficient is defined in equation (11) and is computed as:

$$n_0 = \sum a_n \cos^4 \theta_n \tag{11}$$

With θ_n representing the orientation angle of the printed fiber layers, and a_n indicating the ratio of θ_n - oriented fibers to the total number of printed fibers, the sample studied incorporates a total of 16 fiber layers consisting of 4 layers each at 0°, 45°, -45°, and 90°. So $a_{0^\circ} = a_{45^\circ} = a_{-45^\circ} = a_{90^\circ} = 0.25$ and $n_0 = 0.375$.

3.4.2 Volume Average Stiffness method

The second method is based on the VAS (Volume Average Stiffness) method. This approach presupposes the uniformity of specimen deformation. Multiple sub-steps are necessary to determine the elastic modulus of the composite. First, the stiffness matrices (equations 12 through 14) for the printed fibers, the full pattern (Onyx), and the walls (which we assume to be isotropic) must be computed. These matrices are denoted by Q_{PGF}, Q_{onyx} and Q_{walls}, respectively.

$$Q_{PGF} = \begin{bmatrix} E_{11}/(1-\upsilon_{12}\upsilon_{21}) & \upsilon_{21}E_{11}/(1-\upsilon_{12}\upsilon_{21}) & 0 \\ \upsilon_{12}E_{22}/(1-\upsilon_{12}\upsilon_{21}) & E_{22}/(1-\upsilon_{12}\upsilon_{21}) & 0 \\ 0 & 0 & G_{12} \end{bmatrix} \tag{12}$$

$$Q_{onyx} = \begin{bmatrix} E_o/(1-\upsilon^2) & \upsilon E_o/(1-\upsilon^2) & 0 \\ \upsilon E_o/(1-\upsilon^2) & E_o/(1-\upsilon^2) & 0 \\ 0 & 0 & G_o \end{bmatrix} \tag{13}$$

$$Q_{walls} = \begin{bmatrix} E_w/(1-\upsilon^2) & \upsilon E_w/(1-\upsilon^2) & 0 \\ \upsilon E_w/(1-\upsilon^2) & E_w/(1-\upsilon^2) & 0 \\ 0 & 0 & G_w \end{bmatrix} \tag{14}$$

With E_{11}, E_{22}, υ_{12}, υ_{12}, and G_{12} being the elastic parameters of the printed glass fibers. E_o, υ, and G_o are the elastic parameters of the Onyx. E_w, υ, and G_w are the elastic parameters of the walls. All of these parameters necessary for the calculations have been reported in

Table 4.

The elastic parameters of the printed glass fibers are listed as E_{11}, E_{22}, υ_{12}, υ_{12}, and G_{12}. The Onyx elastic parameters are E_o, υ, and G_o. The elastic parameters of the walls are E_w, υ, and G_w. Table 3 provides an overview of all these parameters.

The stiffness matrix in the global coordinate system for the printed glass fibers $\bar{Q}_{PGF}$ is given by equation (15).

$$\bar{Q}_{PGF} = T Q_{PGF} T^{-1} \tag{15}$$

Where, T is the transformation matrix and is given by expression 16.

$$T = \begin{bmatrix} C^2 & S^2 & 2CS \\ S^2 & C^2 & -2CS \\ -CS & CS & C^2 - S^2 \end{bmatrix} \tag{16}$$

C and S denote the cosine and sine values of the different layers of glass fiber, respectively.

In this study, $Q_{onyx} = \bar{Q}_{onyx}$ and $Q_{walls} = \bar{Q}_{walls}$, as both solid pattern and walls are considered isotropic. The global stiffness matrix ($\bar{Q}$) of the specimen can be calculated from equation (17).

$$\bar{Q} = \bar{Q}_{PGF}V_{PGF} + Q_{onyx}V_{onyx} + Q_{walls}V_{walls} \quad (17)$$

The $\bar{S}_{11}$ matrix (compliance matrix) is calculated as the inverse of the $\bar{Q}$ matrix. The elastic modulus of the specimen is determined through equation (18).

$$E = \frac{1}{\bar{S}_{11}} \quad (18)$$

The stiffness and compliance matrices are calculated using Matlab 2018a software, which leads to calculating the elastic modulus.

3.4.3 Classical Laminate Theory

The third method used for composite calculations is based on classical laminate theory (CLT), which is the most widely used approach. The method requires Equations (19) and (20) to calculate the elastic modulus of the sample.

$$\bar{Q}_{PGF} = T^{-1}Q_{PGF}T^{-T} \quad (19)$$

with T^{-1} representing the inverse of the transformation matrix (T) and T^{-T} representing the inverse of the transpose of the transformation matrix. In this study, $\bar{Q}_{onyx}$ is assumed to be equivalent to Q_{onyx}, as the Onyx layers are isotropic. The stiffness matrix A for the laminate, which comprises glass fiber and Onyx layers, is determined by using the equation (20).

$$A = nfl * [\bar{Q}_{PGF}(0°) + \bar{Q}_{PGF}(45°) + \bar{Q}_{PGF}(-45°) + \bar{Q}_{PGF}(90°)] + nol * \bar{Q}_{onyx} \quad (20)$$

nfl being the number of glass fiber layers per orientation angle, in this study there are 16 glass fiber layers in total so four layers for each orientation ($nfl = 4\ layers$) and nol is the number of Onyx layers, in this study $nol = 28\ layers$. The elastic modulus of the laminate E_1^{Lam} (glass fibers and Onyx layers) can be calculated using expression (21).

$$E_1^{Lam} = \frac{A_{11} * A_{22} - (A_{12})^2}{t * A_{22}} \quad (21)$$

The thickness of the specimen used in this study is $t = 4\ mm$. The elastic modulus of the specimen can be determined by using expression (22) once the elastic modulus of the laminate (E_1^{Lam}) has been calculated.

$$E = V_{lam} * E_1^{Lam} + V_{walls} * E_{walls} \quad (22)$$

With $V_{lam} = V_{PGF} + V_{onyx}$ (23)

With V_{lam} representing the volume of the laminate (made of fiberglass and Onyx) and V_{walls} representing the volume of the walls.

3.4.4 Hart-Smith 10% rule

The final analytical method employed in this study for predicting mechanical properties is based on the 10% method. As per this method, 10% of the composite material's overall stiffness (longitudinal direction) is contributed by fibers oriented at 90° and +/- 45°. Hart-Smith et al. [43] first proposed this method back in 1992, and it is now applied in composite design in the aeronautics industry. Expression (24) is utilized to determine the elastic modulus of the composite material.

$$E = E_{PGF}V_{PGF}\big(0.1 + 0.9 * Rfiber(0°)\big) + E_{onyx}V_{onyx} + E_{walls}V_{walls} \quad (24)$$

In this equation, $Rfiber(0°)$ represents the proportion of fibers at a 0° orientation to the whole number of printed fibers, which, in this study, was equal to 0.25.

3.4.5 Predicted results

All the results obtained by the four methods are plotted in Figure 15, which shows that the analytically predicted values do not disagree with the modulus obtained by tensile testing. The law of mixtures (Krenchel coefficient), the 10% method, and the CLT method underestimate the modulus value, while the VAS method overestimates the modulus value. The prediction errors (error relative to the tensile test) calculated with expression (25) show a difference of 10.48%, 11.83, 6.75%, and 18.25% for the ROM, VAS, CLT, and 10% methods, respectively. The 10% Hart-Smith method induces the largest prediction error compared to the other methods. The difference in results between the modules may be due to the lack of precision in calculating the volume ratios of each component, on the one hand, and to the different assumptions made in applying these analytical calculation methods, on the other hand. Predictive errors found in the literature are comparable to and often much higher than those found in this study. As a point of reference, Lupone et al. [12] recorded prediction errors ranging from 2.2% to 12.4% for the law of mixtures, 0.9% to 8.3% for the VAS method, and 2.3% to 5.9% for the CLT. León-Becerra et al. [44] observed a prediction error of 5.3% when using the VAS method. Based on the acceptable results, these analytical prediction techniques can be used in the 3D printing of long fiber composites to predict mechanical properties for predimensioning and dimensioning purposes.

$$\%Error = \left|\frac{Prediction - Experiment}{Experiment}\right| * 100 \quad (25)$$

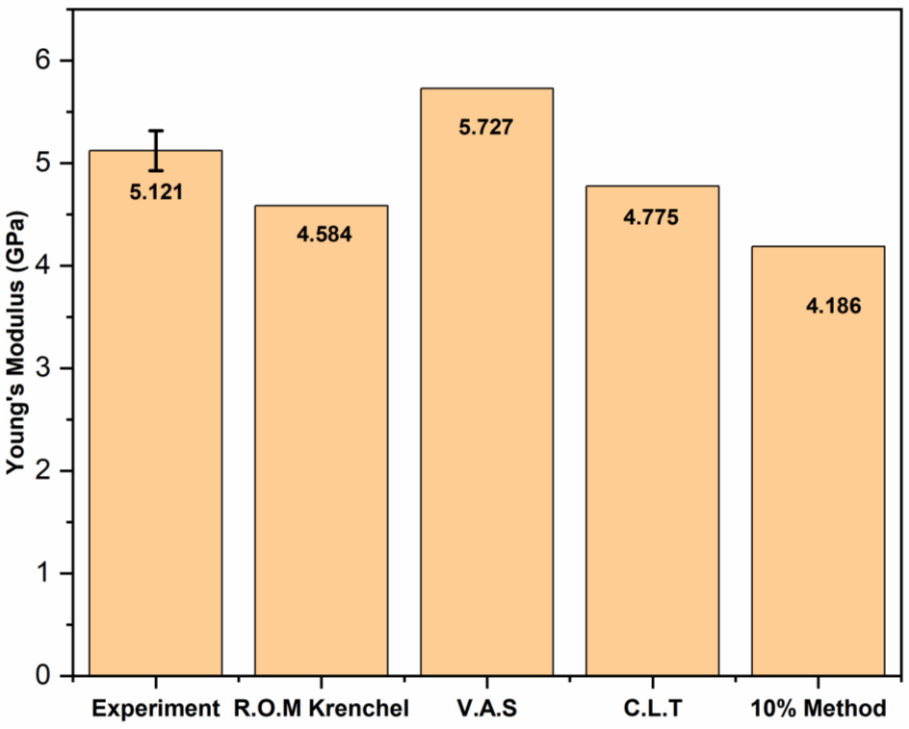

Figure 15: Comparison of the Young's modulus obtained by analytical prediction methods and tensile test.

3.5 Numerical simulation of 3D-printed composite

This study uses numerical simulation to predict the mechanical behavior of tensile-loaded specimens. Two approaches were employed for this purpose: classical numerical simulation of composites using 2D shell elements and numerical simulation using embedded elements. The [0/+45/-45/90]2S

specimen, previously studied, was modeled and simulated using the Abaqus software for both simulations. A specimen containing concentric fibers was simulated using the embedded technique with the objective of predicting the failure zone within the specimen. The properties of the Onyx (infill), walls, and fibers remained identical to those listed in Table 2.

The graphs from the simulations are presented in Figure 16 (a), which illustrate that the embedded element method accurately predicts the entire specimen behavior, unlike the 2D shell model, which only forecasts the elastic region. The distinct Young's modulus calculations derived from experiments and numerical simulations exhibit very close values, as shown in Figure 16 (b). The 2D Shell simulation and embedded elements displayed prediction errors of 7.69% and 4.72%, respectively, compared to the tensile test. These errors are consistent with those observed by Avanzini et al. [32], who found errors ranging from 2.2 - 3.5% and 0.9 - 3.6% for the 2D shell simulation and embedded elements, respectively. When the experimental specimen reaches its failure load, the simulation shows maximum stresses of 81 MPa and 3350 MPa for the matrix (Onyx) and fibers, respectively (Figure 17 (a and b)). The Onyx's stress level indicates plasticization, and according to El-Wazery et al. [39], the tensile strength of glass fibers is around 3400 MPa, suggesting that the fibers (mainly the longitudinal ones) likely failed. The study's matrix (Onyx) modeling differentiates between the infill pattern (solid) and the walls, which exhibit distinct mechanical behaviors explained by a preceding study [42]. This differentiation results in an enhanced prediction of the stress field in the matrix.

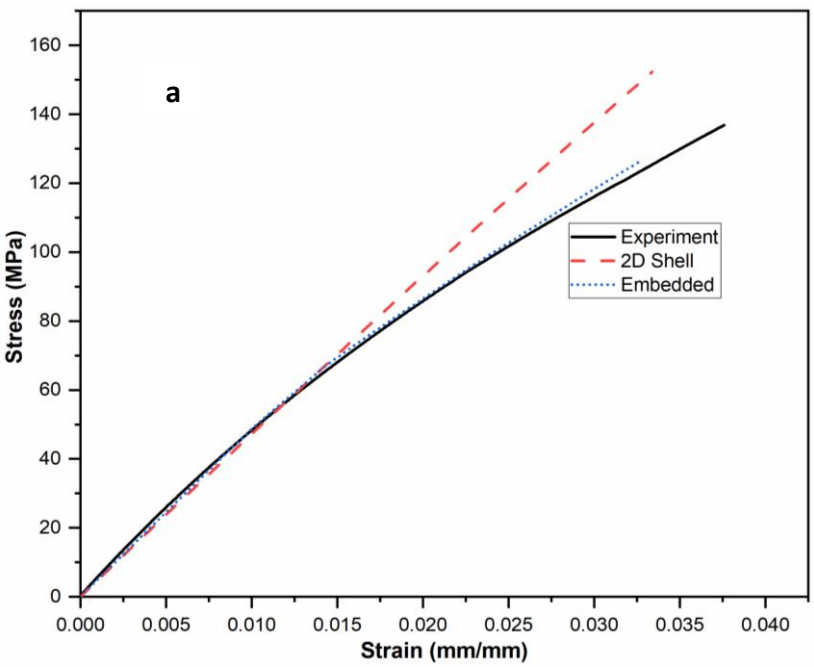

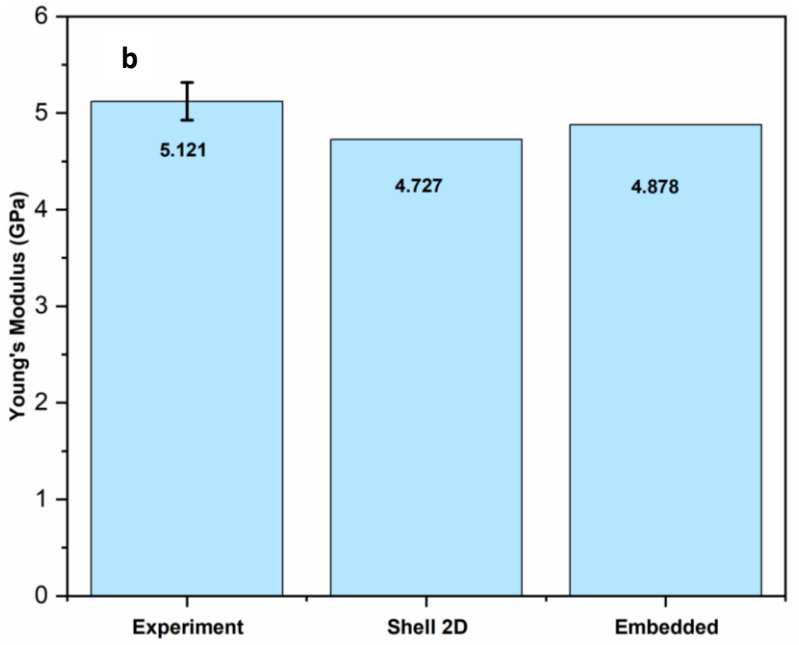

Figure 16: Comparison between experiment and numerical simulations: a) tensile test curves; b) Young's modulus.

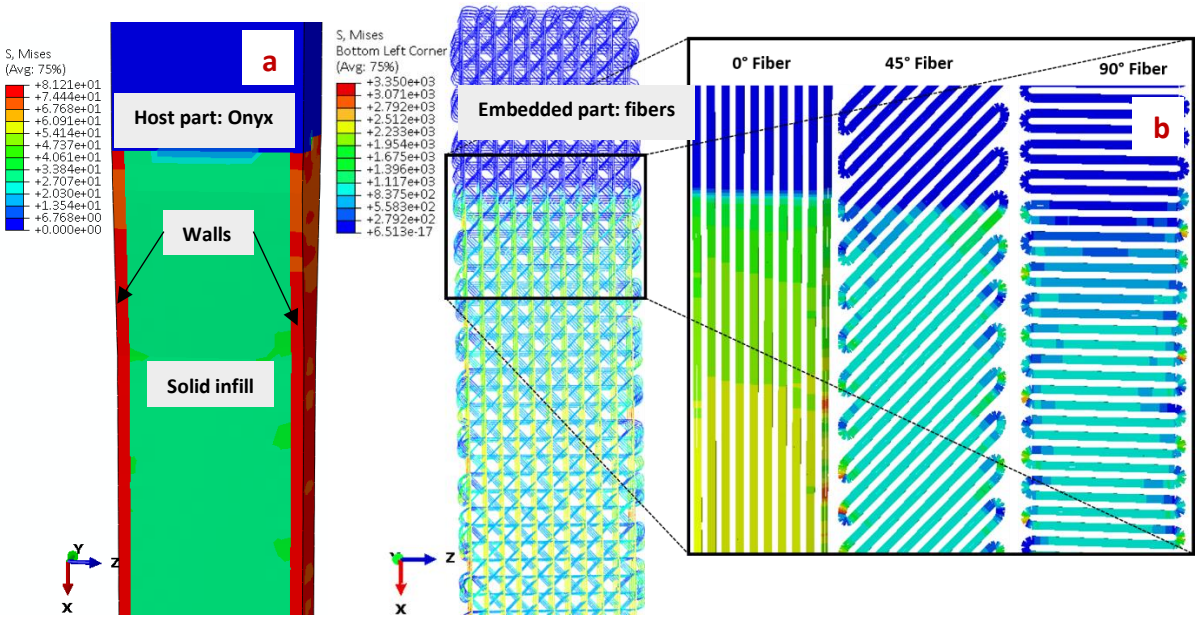

Figure 17: Von Mises stress maps for Onyx and fibers part: a) Onyx part (solid infill and walls part); b) fibers part (0°, 45° and 90° fibers).

Simulation can predict the mechanical properties of specimens with concentric fibers. However, conventional 2D shell element simulation of composites is limited in predicting the overall behavior of concentric and isotropic specimens. Embedded elements can predict the overall behavior and probable failure zones of specimens with concentric fibers, as shown in Figure 18. One benefit of this modeling method is its ability to replicate the fiber trajectory and provide a more accurate prediction of mechanical behavior, as depicted in Figure 16 (a). In contrast, 2D shell simulations merely forecast the purely elastic behavior of the specimen. Incorporating a fiber fracture model could have been considered to enhance the simulation's realism in the context of tensile testing.

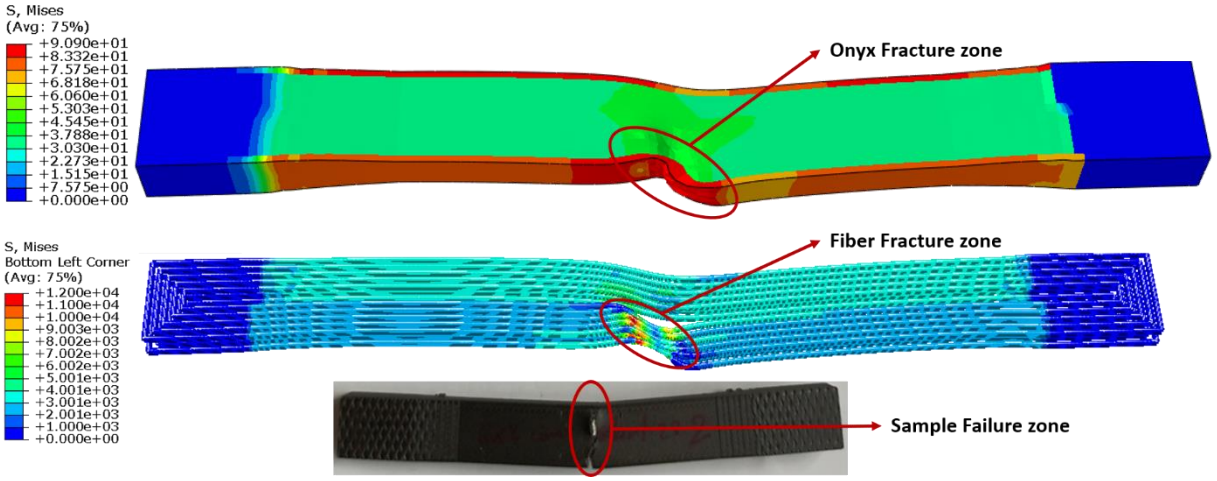

Figure 18: Comparison of the fracture zone of the tested sample and numerical simulation (Concentric sample, Start rotation2).

One limitation of the embedded element method involves overestimating mass and stiffness in studied specimens. This may result in inaccurate predictions within certain simulations, such as fatigue, modal, or dynamic. Additionally, the inability to manage matrix/fiber bonding utilizing cohesive elements represents another limitation of this technique. The numerical method has limited availability in simulation software packages, including Abaqus, and is exclusively applicable to finite elements (host elements) with no rotational degrees of freedom. Nevertheless, this method is still a trustworthy and practical approach for predicting the behavior and mechanical properties of 3D-printed composites, especially when the fiber trajectory follows a complex shape, such as the case presented in the work of Zhang et al. [45].

3.6 Towards optimizing composite 3D printing

Optimizing print parameters allows 3D printer users to reduce raw material consumption (plastics and fibers), costs, and printing time. In this section, we explore how to optimize these parameters while considering mechanical properties. This necessitates discovering a balance between the Young's modulus, printing time, and material cost. The previously observed specimen ([0/+45/-45/90]2S) will be utilized for this examination. In 3D printing, the cost of glass fibers is higher than that of Onyx, and parts with a higher number of walls require more printing time. To decrease the volume of glass fibers used and printing costs while concentrating on the Young's modulus and printing time, the aim is to increase the number of walls in the specimen. It is known that walls have a high Young's modulus (approx. 5400 MPa). The issue at hand can be efficiently summarized through a function where the primary variable is the number of walls, and the outcomes are the Young's modulus, printing cost, and time, as demonstrated in equation (26).

$$f(walls) = E, time, cost \tag{26}$$

The findings demonstrate a correlation between an increase in the number of walls and printing time and a decrease in material costs (Figure 19). Increasing the number of walls reduces the volume of the fibers, resulting in a lower final cost of the specimen as the cost of fibers is higher than that of Onyx. The compromise attained through the analyses is a Young's modulus of 5300 MPa, a printing duration of 99 minutes, and a cost of $3.15. For large-scale manufacturing, conducting a study of this nature could result in considerable reductions in printing time and cost while maintaining acceptable mechanical properties.

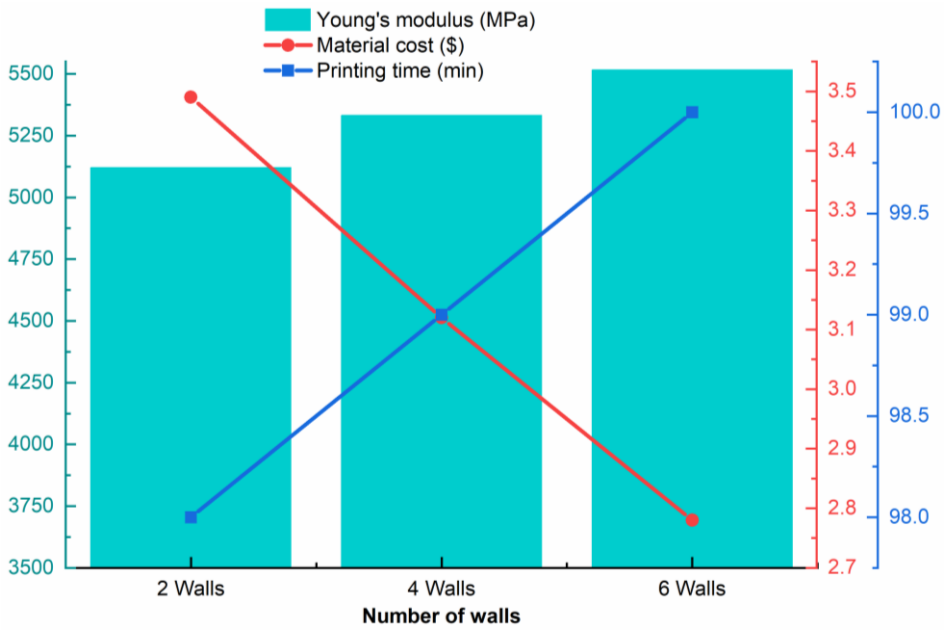

Figure 19: Optimization of the Young's modulus according to printing time, cost, and number of walls.

4 Conclusion

The present study investigates the mechanical properties of Onyx samples reinforced with continuous glass fibers. Various printing parameters for glass fibers were analyzed, and experimental, analytical, and numerical investigations were conducted to predict the mechanical behavior of printed parts. The study's main conclusions are as follows:

1- Considering the fiber printing parameters, block printing of the fibers in the composite offers better mechanical performance than alternating fiber printing with Onyx. The start rotation, which marks the beginning of concentric fiber printing, is a crucial parameter to consider when designing and parameterizing part printing. Improper adjustment of this parameter, particularly if it is located in a useful area of the printed parts, can result in premature part breakage.

2- The prediction of the elastic modulus of Onyx/fiberglass specimens resulted in acceptable prediction errors ranging from 6.75% to 18.25%. This level of accuracy was achieved by taking into account the different sections of the specimens, including walls, patterns, and fibers, and estimating the equivalent volume ratios for each section.

3- Numerical simulation with embedded elements is an effective method for predicting the behavior and mechanical properties of 3D-printed composites. The observed prediction error is 4.7%. This technique accurately predicts the behavior and potential failure zones of specimens composed of concentric fibers. Compared to conventional 2D shell element simulation, this technique offers greater efficiency. However, this method appears to be unavailable in most commercial numerical simulation software, which restricts its use in research and engineering by the majority.

In conclusion, selecting the appropriate printing parameters is crucial for obtaining mechanically reliable 3D-printed composite parts. Traditional tools can be used to predict mechanical properties and behavior analytically and numerically. The results presented in this article may enhance the development of practical applications achieved through continuous-fiber composite 3D printing.

Declaration of Competing Interest

The authors declare that they have no known competing financial interests or personal relationships that could have influenced the work reported in this paper.

Credit authorship contribution statement

Daouda Nikiema: Conceptualization, writing, review, and editing; **Pascale Balland**: Resources, Funding acquisition, writing, review, and editing; **Alain Sergent**: Writing, review, and editing;

Data availability

Data will be made available on request.

Acknowledgment

Daouda NIKIEMA reports writing assistance was provided by the University Savoie Mont Blanc Laboratory of Systems and Materials for Mechatronics.

References

[1] R.C. Advincula, J.R.C. Dizon, Q. Chen, I. Niu, J. Chung, L. Kilpatrick, R. Newman, Additive manufacturing for COVID-19: Devices, materials, prospects, and challenges, MRS Commun. 10 (2020) 413–427. https://doi.org/10.1557/mrc.2020.57.

[2] Sculpteo, The state of 3D PRINTING: The data you need to understand the 3D Printing world and build your 3D Printing strategy, Print. Polym. Fundam. Appl. (2015) 293–306.

[3] S.A.M. Tofail, E.P. Koumoulos, A. Bandyopadhyay, S. Bose, L. O'Donoghue, C. Charitidis, Additive manufacturing: scientific and technological challenges, market uptake and opportunities, Mater. Today. 21 (2018) 22–37. https://doi.org/10.1016/j.mattod.2017.07.001.

[4] R. Surya Teja, M. Lokesh, S. Deepak Kumar, P.S.V. Ramana Rao, 3D Printing of complex structures: Case study of Eiffel Tower, Mater. Today Proc. (2022). https://doi.org/10.1016/j.matpr.2022.12.037.

[5] F. Pahlevanzadeh, H.R. Bakhsheshi-Rad, D. Brabazon, M. Kharaziha, A.F. Ismail, S. Sharif, M. Razzaghi, F. Berto, Additive Manufacturing of Polymer Matrix Composites, Encycl. Mater. Compos. (2021) 1013–1028. https://doi.org/10.1016/B978-0-12-819724-0.00025-2.

[6] I. Blanco, The use of composite materials in 3d printing, J. Compos. Sci. 4 (2020). https://doi.org/10.3390/jcs4020042.

[7] S. Kumar, I. Singh, S.S. R. Koloor, D. Kumar, M.Y. Yahya, On Laminated Object Manufactured FDM-Printed ABS/TPU Multimaterial Specimens: An Insight into Mechanical and Morphological Characteristics, Polymers (Basel). 14 (2022). https://doi.org/10.3390/polym14194066.

[8] M. Manoj Prabhakar, A.K. Saravanan, A. Haiter Lenin, I. Jerin leno, K. Mayandi, P. Sethu Ramalingam, A short review on 3D printing methods, process parameters and materials, Mater. Today Proc. (2020). https://doi.org/10.1016/j.matpr.2020.10.225.

[9] S. Kumar, R. Singh, M. Singh, T.P. Singh, A. Batish, Multi material 3D printing of PLA-PA6/TiO2 polymeric matrix: Flexural, wear and morphological properties, J. Thermoplast. Compos. Mater. 35 (2020) 2105–2124. https://doi.org/10.1177/0892705720953193.

[10] S. Kumar, I. Singh, D. Kumar, J. Mago, S.S.R. Koloor, Mechanical, morphological, and dimensional properties of heat-treated fused deposition modeling printed polymeric matrix of polyethylene terephthalate glycol, Prog. Rubber, Plast. Recycl. Technol. 0 (n.d.) 14777606231218354. https://doi.org/10.1177/14777606231218354.

[11] S. Kumar, R. Singh, T.P. Singh, A. Batish, M. Singh, Multi-stage Primary and Secondary Recycled PLA Composite Matrix for 3D Printing Applications, Proc. Natl. Acad. Sci. India Sect. A Phys. Sci. 92 (2022) 677–698. https://doi.org/10.1007/s40010-022-00783-y.

[12] F. Lupone, E. Padovano, C. Venezia, C. Badini, Experimental Characterization and Modeling of 3D Printed Continuous Carbon Fibers Composites with Different Fiber Orientation Produced by FFF Process, Polymers (Basel). 14 (2022). https://doi.org/10.3390/polym14030426.

[13] R.R. Fernandes, A.Y. Tamijani, M. Al-Haik, Mechanical characterization of additively manufactured fiber-reinforced composites, Aerosp. Sci. Technol. 113 (2021) 106653. https://doi.org/10.1016/j.ast.2021.106653.

[14] B. Brenken, E. Barocio, A. Favaloro, R.B. Pipes, V. Kunc, Fused fi lament fabrication of fi ber-reinforced polymers : A review, 21 (2018) 1–16.

[15] X. Tian, A. Todoroki, T. Liu, L. Wu, Z. Hou, M. Ueda, Y. Hirano, R. Matsuzaki, K. Mizukami, K. Iizuka, A. V. Malakhov, A.N. Polilov, D. Li, B. Lu, 3D Printing of Continuous Fiber Reinforced

Polymer Composites: Development, Application, and Prospective, Chinese J. Mech. Eng. Addit. Manuf. Front. 1 (2022) 100016. https://doi.org/10.1016/j.cjmeam.2022.100016.

[16] F.P.G. J. Justo, L. Távara∗, L. García-Guzmán, Characterization of 3D printed long fibre reinforced composites, (2018) 537–548. https://doi.org/10.1016/j.compstruct.2017.11.052.

[17] H. Al Abadi, H.T. Thai, V. Paton-Cole, V.I. Patel, Elastic properties of 3D printed fibre-reinforced structures, Compos. Struct. 193 (2018) 8–18. https://doi.org/10.1016/j.compstruct.2018.03.051.

[18] S.M.F. Kabir, K. Mathur, A.F.M. Seyam, A critical review on 3D printed continuous fiber-reinforced composites: History, mechanism, materials and properties, Compos. Struct. 232 (2020) 1–24. https://doi.org/10.1016/j.compstruct.2019.111476.

[19] L. Li, W. Liu, L. Sun, Mechanical characterization of 3D printed continuous carbon fiber reinforced thermoplastic composites, 227 (2022).

[20] Y. Chen, Z. Shan, X. Yang, Y. Song, A. Zou, Preparation of CCF/PEEK filaments together with property evaluation for additive manufacturing, Compos. Struct. 281 (2022). https://doi.org/10.1016/j.compstruct.2021.114975.

[21] K. Saeed, A. McIlhagger, E. Harkin-Jones, C. McGarrigle, D. Dixon, M. Ali Shar, A. McMillan, E. Archer, Characterization of continuous carbon fibre reinforced 3D printed polymer composites with varying fibre volume fractions, Compos. Struct. 282 (2022). https://doi.org/10.1016/j.compstruct.2021.115033.

[22] Z. Ali, Y. Yan, H. Mei, L. Cheng, L. Zhang, Effect of infill density, build direction and heat treatment on the tensile mechanical properties of 3D-printed carbon-fiber nylon composites, Compos. Struct. 304 (2023). https://doi.org/10.1016/j.compstruct.2022.116370.

[23] S.H.R. Sanei, D. Popescu, 3d-printed carbon fiber reinforced polymer composites: A systematic review, J. Compos. Sci. 4 (2020). https://doi.org/10.3390/jcs4030098.

[24] S.M.F. Kabir, K. Mathur, A.F.M. Seyam, Impact resistance and failure mechanism of 3D printed continuous fiber-reinforced cellular composites, J. Text. Inst. 112 (2021) 752–766. https://doi.org/10.1080/00405000.2020.1778223.

[25] S.H.R. Sanei, A. Arndt, R. Doles, Open hole tensile testing of 3D printed continuous carbon fiber reinforced composites, J. Compos. Mater. 54 (2020) 2687–2695. https://doi.org/10.1177/0021998320902510.

[26] T. Yu, Z. Zhang, S. Song, Y. Bai, D. Wu, Tensile and flexural behaviors of additively manufactured continuous carbon fiber-reinforced polymer composites, Compos. Struct. 225 (2019). https://doi.org/10.1016/j.compstruct.2019.111147.

[27] M. Mohammadizadeh, A. Imeri, I. Fidan, M. Elkelany, 3D printed fiber reinforced polymer composites - Structural analysis, Compos. Part B Eng. 175 (2019). https://doi.org/10.1016/j.compositesb.2019.107112.

[28] J.G. Díaz-Rodríguez, A.D. Pertúz-Comas, O.A. González-Estrada, Mechanical properties for long fibre reinforced fused deposition manufactured composites, Compos. Part B Eng. 211 (2021). https://doi.org/10.1016/j.compositesb.2021.108657.

[29] J. Naranjo-Lozada, H. Ahuett-Garza, P. Orta-Castañón, W.M.H. Verbeeten, D. Sáiz-González, Tensile properties and failure behavior of chopped and continuous carbon fiber composites produced by additive manufacturing, Addit. Manuf. 26 (2019) 227–241. https://doi.org/10.1016/j.addma.2018.12.020.

[30] N. van de Werken, J. Hurley, P. Khanbolouki, A.N. Sarvestani, A.Y. Tamijani, M. Tehrani, Design considerations and modeling of fiber reinforced 3D printed parts, Compos. Part B Eng. 160 (2019) 684–692. https://doi.org/10.1016/j.compositesb.2018.12.094.

[31] D. Krzikalla, J. Měsíček, R. Halama, J. Hajnyš, M. Pagáč, T. Čegan, J. Petrů, On flexural properties of additive manufactured composites: Experimental, and numerical study, Compos. Sci. Technol. 218 (2022). https://doi.org/10.1016/j.compscitech.2021.109182.

[32] A. Avanzini, D. Battini, L. Giorleo, Finite element modelling of 3D printed continuous carbon fiber composites: Embedded elements technique and experimental validation, Compos. Struct. 292 (2022). https://doi.org/10.1016/j.compstruct.2022.115631.

[33] D.R. Hetrick, S.H.R. Sanei, C.E. Bakis, O. Ashour, Evaluating the effect of variable fiber content on mechanical properties of additively manufactured continuous carbon fiber composites, J. Reinf. Plast. Compos. 40 (2021) 365–377. https://doi.org/10.1177/0731684420963217.

[34] D. Nikiema, P. Balland, A. Sergent, Experimental and numerical investigations of 3D-printed Onyx parts reinforced with continuous glass fibers, Arch. Civ. Mech. Eng. 24 (2024) 50. https://doi.org/10.1007/s43452-024-00861-5.

[35] L. Marşavina, C. Vălean, M. Mărghitaş, E. Linul, N. Razavi, F. Berto, R. Brighenti, Effect of the manufacturing parameters on the tensile and fracture properties of FDM 3D-printed PLA specimens, Eng. Fract. Mech. 274 (2022). https://doi.org/10.1016/j.engfracmech.2022.108766.

[36] D.R. Hetrick, S.H.R. Sanei, O. Ashour, C.E. Bakis, Charpy impact energy absorption of 3D printed continuous Kevlar reinforced composites, J. Compos. Mater. 55 (2021) 1705–1713. https://doi.org/10.1177/0021998320985596.

[37] R. Delbart, A. Papasavvas, C. Robert, T. Quynh Truong Hoang, F. Martinez-Hergueta, An experimental and numerical study of the mechanical response of 3D printed PLA/CB polymers, Compos. Struct. (2023) 117156. https://doi.org/10.1016/j.compstruct.2023.117156.

[38] C. Pascual-González, M. Iragi, A. Fernández, J.P. Fernández-Blázquez, L. Aretxabaleta, C.S. Lopes, An approach to analyse the factors behind the micromechanical response of 3D-printed composites, Compos. Part B Eng. 186 (2020). https://doi.org/10.1016/j.compositesb.2020.107820.

[39] M.S. El-Wazery, M.I. El-Elamy, S.H. Zoalfakar, Mechanical Properties of Glass Fiber Reinforced Polyester Composites, Int. J. Appl. Sci. Eng. 14 (2017) 121. https://doi.org/10.6703/IJASE.2017.14(3).121.

[40] G.W. Melenka, B.K.O. Cheung, J.S. Schofield, M.R. Dawson, J.P. Carey, Evaluation and prediction of the tensile properties of continuous fiber-reinforced 3D printed structures, Compos. Struct. 153 (2016) 866–875. https://doi.org/10.1016/j.compstruct.2016.07.018.

[41] G.D. Goh, V. Dikshit, A.P. Nagalingam, G.L. Goh, S. Agarwala, S.L. Sing, J. Wei, W.Y. Yeong, Characterization of mechanical properties and fracture mode of additively manufactured carbon fiber and glass fiber reinforced thermoplastics, Mater. Des. 137 (2018) 79–89. https://doi.org/10.1016/j.matdes.2017.10.021.

[42] D. Nikiema, N.A. Sène, P. Balland, A. Sergent, Study of walls' influence on the mechanical properties of 3D printed onyx parts: Experimental, analytical and numerical investigations, Heliyon. 9 (2023) e19187. https://doi.org/10.1016/j.heliyon.2023.e19187.

[43] L. ~J. Hart-Smith, The ten-percent rule for preliminary sizing of fibrous composite structures, Weight Eng. 52 (1992) 29–45.

[44] J.S. León-Becerra, O.A. González-Estrada, W. Pinto-Hernández, Mechanical characterization of additive manufacturing composite parts, Respuestas. 25 (2020). https://doi.org/10.22463/0122820x.2189.

[45] H. Zhang, S. Wang, K. Zhang, J. Wu, A. Li, J. Liu, D. Yang, 3D printing of continuous carbon fibre reinforced polymer composites with optimised structural topology and fibre orientation, Compos. Struct. (2023) 116914. https://doi.org/10.1016/j.compstruct.2023.116914.